

NASA

MEMORANDUM

EFFECT OF HORIZONTAL-TAIL CHORD ON THE CALCULATED
SUBSONIC SPAN LOADS AND STABILITY DERIVATIVES
OF ISOLATED UNSWEPT TAIL ASSEMBLIES IN
SIDESLIP AND STEADY ROLL

By Katherine W. Booth

Langley Research Center
Langley Field, Va.

**NATIONAL AERONAUTICS AND
SPACE ADMINISTRATION**

WASHINGTON
March 1959

NATIONAL AERONAUTICS AND SPACE ADMINISTRATION

MEMORANDUM 4-1-59L

EFFECT OF HORIZONTAL-TAIL CHORD ON THE CALCULATED
SUBSONIC SPAN LOADS AND STABILITY DERIVATIVES
OF ISOLATED UNSWEPT TAIL ASSEMBLIES IN
SIDESLIP AND STEADY ROLL

By Katherine W. Booth

SUMMARY

Subsonic span loads and the resulting stability derivatives have been calculated using the discrete-horseshoe-vortex method for a systematic series of horizontal tails in combination with a vertical tail of aspect ratio 1.0 in order to provide information on the effect of varying the chord of the horizontal tail for isolated tail assemblies performing sideslip and steady-roll motions. In addition, the effects of horizontal-tail dihedral angle for the sideslip case were obtained. Each tail surface considered had a taper ratio of 0.5 and an unswept quarter-chord line. The investigation covered variations in horizontal-tail chord, horizontal-tail span, and vertical location of the horizontal tail. The span loads and the resulting total stability derivatives as well as the vertical- and horizontal-tail contributions to these tail-assembly derivatives are presented in the figures for the purpose of showing the influence of the geometric variables.

The results of this investigation showed trends that were in agreement with the results of previous investigations for variations in horizontal-tail span and vertical location of the horizontal tail. Variations in horizontal-tail chord expressed herein in terms of the root-chord ratio, that is, the ratio of horizontal-tail root chord to vertical-tail root chord, were found to have a pronounced influence on most of the span loads and the resulting stability derivatives. For most of the cases considered, the rate of change of the span load coefficients and the stability derivatives with the root-chord ratio was found to be a maximum for small values of root-chord ratio and to decrease as root-chord ratio increased.

INTRODUCTION

Accurate information on the magnitude and distribution of tail loads is important in estimating the contribution of tail assemblies to the aerodynamic derivatives of complete airplane configurations and for the structural design of the tail assembly. For the subsonic-speed range, information on tail loads for a variety of isolated intersecting vertical- and horizontal-tail configurations performing various motions is available. (For example, see refs. 1 to 4.) However, theoretical analyses have considered only configurations for which the vertical- and horizontal-tail root chords are equal. The purpose of the present paper is to provide some information concerning the influence of varying the length of the horizontal-tail chord on the span loads and the resulting stability derivatives for isolated unswept tail assemblies in sideslip and steady roll. In addition, the incremental span loads due to dihedral of the horizontal-tail surfaces are determined for the sideslip case. Calculations are made using the discrete-horseshoe-vortex method (refs. 4 to 6) for a single unswept vertical surface of aspect ratio 1.0 and taper ratio 0.5 in combination with unswept horizontal surfaces having taper ratios of 0.5 and various root chords, semispans, and vertical positions relative to the vertical tail.

SYMBOLS

The results presented herein are referred to the stability system of axes with the origin at the quarter-chord of the vertical-tail root chord. (See fig. 1.)

A	aspect ratio, b^2/S
b	span, ft
S	area, sq ft
c	local chord, ft
\bar{c}	average geometric chord, ft
c_r	root chord, ft
$\frac{c_{r,h}}{c_{r,v}}$	root-chord ratio

ρ	mass density of air, slugs/cu ft
V	free-stream velocity, ft/sec
β	sideslip angle, radians
Γ	dihedral angle of horizontal tail, radians
x, y, z	coordinate distances relative to stability system of axes
p	rate of roll, radians/sec
C_Y	lateral-force coefficient, $\frac{\text{Lateral force}}{\frac{1}{2} \rho V^2 S_v}$
C_l	rolling-moment coefficient, $\frac{\text{Rolling moment}}{\frac{1}{2} \rho V^2 S_v b_v}$
c_l	section-lift coefficient, $\frac{\text{Section lift}}{\frac{1}{2} \rho V^2 c}$

$$C_{Y\beta} = \frac{\partial C_Y}{\partial \beta}$$

$$C_{l\beta} = \frac{\partial C_l}{\partial \beta}$$

$$\frac{C_{Y\beta}}{\Gamma} = \frac{\partial C_{Y\beta}}{\partial \Gamma}$$

$$\frac{C_{Y\beta}}{\Gamma^2} = \frac{\partial C_{Y\beta}}{\partial \Gamma^2}$$

$$\frac{C_{l\beta}}{\Gamma} = \frac{\partial C_{l\beta}}{\partial \Gamma}$$

$$C_{Yp} = \frac{\partial C_Y}{\partial \frac{pb_v}{V}}$$

$$C_{l_p} = \frac{\partial C_l}{\partial \frac{pb_v}{V}}$$

Subscripts:

h horizontal tail

v vertical tail

Subscripts used in the span load coefficients, such as $\frac{(cc_l)_h}{\bar{c}_v \beta}$, signify that \bar{c} is the average geometric chord of the vertical tail and that c_l and the chord c are based on horizontal-tail geometry.

PRELIMINARY REMARKS

The basic finite-step method used herein is the same as that used in reference 4 and is an adaptation of the method applied in reference 6 to the computation of wing loads. The theoretical considerations involved in applying this method to intersecting surfaces are not included in this paper since they are presented in appendix A of reference 4.

For all tail configurations considered in this paper, the vertical tail is represented by 6 equispan horseshoe vortices and the horizontal tail by 12 equispan horseshoe vortices. (See fig. 2.) Therefore, each tail combination is represented by a total of 18 horseshoe vortices which result in a set of 18 simultaneous equations with 18 unknown vortex strengths. When motions such as rolling and sideslip are considered, the horizontal-tail loads are antisymmetric (equal but of opposite sign on each panel); therefore, the number of equations may be reduced to 12. All solutions of the simultaneous equations were obtained by use of a relay-type computer.

Mach number effects were not taken into account, and vertical displacement of the vortices of the horizontal tail due to dihedral angle was neglected. The angles β , Γ , and $\frac{pb_v}{V}$ are assumed to be sufficiently small so that the sine of the angle can be replaced by the angle in radians and the cosine, by 1.0. All calculations were made for a two-dimensional lift-curve slope of 2π .

SCOPE

Calculations were made for a systematic series of isolated tail assemblies performing sideslip and steady-roll motions. For these two motions, three basic span loads, two resulting from the sideslip motion and one from the steady-roll motion, were obtained. The three cases considered are:

(1) Loads resulting from sideslipping the tail combinations having horizontal tails with zero dihedral.

(2) Incremental loads resulting from sideslipping the horizontal tails having dihedral angle.

(3) Loads resulting from rolling the tail combinations about an axis coincident with the root chord of the vertical tail.

The loads calculated for case (2) should be considered as additional loads due to horizontal-tail dihedral angle. For the small angles considered herein, it is assumed that the total load in sideslip on any tail combination having dihedral can be obtained by the proper addition of the loads obtained from case (1) and case (2). In all three cases, the additional restriction that the horizontal surface remains at zero geometric angle of attack was imposed.

Span loads and the resulting stability derivatives are presented for unswept tail configurations having a single vertical surface of aspect ratio 1.0 and a taper ratio of 0.5 in combination with a number of horizontal surfaces, with each horizontal surface having a taper ratio of 0.5. Horizontal tails having spans b_h of $\frac{4}{3}b_v$, $\frac{8}{3}b_v$, and $4b_v$ were considered at three vertical locations, at the base, at the mid position, and at the top of the vertical tail. For each span, the horizontal-tail chord was varied and, since only horizontal tails of 0.5 taper ratio were considered, the variation in horizontal-tail chord was expressed herein as a variation in root-chord ratio $\frac{c_{r,h}}{c_{r,v}}$. Calculations were performed for values of root-chord ratio $\frac{c_{r,h}}{c_{r,v}}$ of 0, 1/4, 1/2, 3/4, and 1.0. For all cases, the quarter-chord of the horizontal-tail root chord intersected the vertical-tail quarter-chord line. Sketches showing the plan forms covered in this investigation are presented in table I.

PRESENTATION OF RESULTS

The results of the investigation are presented in two main groups, the first group containing span loads (figs. 3 to 5) and the second group containing stability derivatives (figs. 6 to 11). In figures 3 to 5, negative values of the vertical-tail load coefficient indicate a negative lateral force. The horizontal-tail load coefficients are for the right (positive) semispan facing into the wind, and positive values signify lift loads. Loads on the left semispan of the horizontal tail are equal in magnitude but opposite in sign to the loads on the right semispan for the corresponding spanwise station.

All derivatives are based on the geometry of the vertical tail in order to indicate the relative magnitudes of the vertical- and horizontal-tail contributions to the total derivative for a given tail configuration. In order to indicate the influence of the horizontal-tail chord, all derivatives are plotted against root-chord ratios. (The horizontal tails and the vertical tail have a taper ratio of 0.5.)

RESULTS AND DISCUSSION

Span Load Distributions

Sideslip without dihedral.- The span loads due to sideslip on unswept tail assemblies having horizontal tails of zero geometric dihedral are presented in figure 3. The vertical-tail span loads presented in figure 3(a) show that changes in root-chord ratio can provide significant changes in the magnitude of the end-plate effect when the root-chord ratio has a value of 0.5 or less. For horizontal tails located at the middle of the vertical tail, the calculations show no noticeable effect of root-chord ratio on the vertical-tail span load.

The nondimensional span load coefficients for the induced loading on the horizontal tails are presented in figure 3(b). As expected, this figure indicates that for horizontal tails of given span located at either extremity of the vertical tail an increase in the root-chord ratio produced an increase in the magnitude of the induced load on the horizontal tails. An examination of the values of the horizontal-tail span load coefficient for the low and high positions indicates that a large percentage of the induced load shown for a value of $\frac{c_{r,h}}{c_{r,v}}$ of 1.0 was obtained for a root-chord ratio of 0.5. This effect of root-chord ratio is, in addition, influenced by horizontal-tail span as evidenced by the

fact that the rate of change of span load coefficient is almost linear with root-chord ratio over the outboard portion of the largest span horizontal tails. Figure 3(b) also indicates that the effect of horizontal-tail position and horizontal-tail span are consistent with those shown in reference 4. The negligibly small induced loads shown for horizontal tails in the mid position are due directly to the effect of vertical-tail taper.

The span loads presented in figure 3(b) are for the right semispan of the horizontal tail. Since the loads on the left semispan are equal in magnitude but opposite in sign, there results for the complete horizontal tail a zero lift force and a rolling moment about the root chord of the horizontal tail.

Sideslip of horizontal tails with dihedral.- The induced span loads of the vertical tail due to the horizontal-tail dihedral angle are presented in figure 4(a). For horizontal tails located at all three vertical locations, figure 4(a) indicates that the rate of change of span load coefficient with root-chord ratio is small above root-chord-ratio values of about 0.5. Also apparent is the increase in the magnitude of the induced load with an increase in horizontal-tail span. The effect of horizontal-tail position is directly associated with the reversed direction of the induced load on the vertical tail for portions of the vertical tail above and below the horizontal tail. The effects of horizontal-tail span and position are, of course, similar to those shown in reference 4.

The span loads on the horizontal tails due to horizontal-tail dihedral angle are presented in figure 4(b). The effect of root-chord ratio was about as expected; that is, the span load coefficients show an increase for an increase in root-chord ratio. Calculations were not made on the isolated horizontal tails for the additional load due to dihedral angle; however, span loads are presented in reference 4 for isolated horizontal tails with dihedral, ranging in aspect ratio from 1 to 9, having unswept quarter-chord lines, and a taper ratio of 0.50.

Steady roll.- Calculated span load distributions on the vertical and horizontal surfaces for tail assemblies in steady roll about an axis coincident with the vertical-tail root chord are presented in figure 5. The results indicate that root-chord ratio $\frac{c_{r,h}}{c_{r,v}}$ as well as horizontal-tail span and vertical location of the horizontal tail have a large influence on the vertical-tail span load. (See fig. 5(a).) An examination of the vertical-tail span load coefficients indicates that, in general, increasing root-chord ratio or horizontal-tail span produces an increase in the span load for those portions of the vertical tail below the horizontal tail and a decrease in the span load for those portions

above the horizontal tail as compared to the span load of the vertical tail alone. In summary, root-chord ratio and horizontal-tail span affect only the magnitude of the span load coefficients, whereas horizontal-tail position determines the overall shape of the load distribution on the vertical tail.

Of particular interest in figure 5(a) is the negligible effect of root-chord ratio for configurations having the shortest span horizontal tail in the low position. For these configurations, the increase in vertical-tail load due to end-plate effect was almost cancelled by that load induced on the vertical tail by the horizontal-tail rolling load. For configurations having the larger span horizontal tails in the low position, a reversal in the direction of load occurred over a considerable portion of the vertical-tail span when the root-chord ratio was greater than about 0.5. A similar reversal can occur for horizontal tails in the mid position as indicated for the configuration having $\frac{b_h}{b_v} = 4$ and $\frac{c_{r,h}}{c_{r,v}} = 1$.

The horizontal-tail span loads for the various tail assemblies in steady roll are presented in figure 5(b). In general, the loads on the horizontal tail increase with an increase in root-chord ratio and with an increase in horizontal-tail span. Vertical location of the horizontal tail also affects the span loads on the horizontal tail, particularly in the region near the vertical tail. This influence can be seen by noting the values of the span load coefficients at the root chord of the horizontal tail for the low and high positions. In fact, for the low position a reversal in the direction of load is indicated for the region near the vertical tail for the shortest horizontal-tail span considered.

Stability Derivatives

Sideslip without dihedral.- The lateral-force and rolling-moment stability derivatives $C_{Y\beta}$ and $C_{l\beta}$ are obtained from an integration of the span load distributions. Since the dihedral angle is zero for the horizontal tail, $C_{Y\beta}$ results only from the vertical-tail load. However, $C_{l\beta}$ is composed of contributions from both the vertical- and horizontal-tail loads and represents, of course, the result for the complete-tail configuration. The separate contributions of the vertical and horizontal tails $(C_{l\beta})_v$ and $(C_{l\beta})_h$, respectively, are also presented.

The variations of $C_{Y\beta}$ with root-chord ratio $\frac{c_{r,h}}{c_{r,v}}$ for the various tail assemblies are presented in figure 6. Locating the horizontal tails at either extremity of the vertical tail produced similar variations of $C_{Y\beta}$ with root-chord ratio. Most of the available increase in $C_{Y\beta}$ for horizontal tails in these two locations was obtained when the root-chord ratio was increased from 0 to 0.50 and when the horizontal-tail span had a value of $b_h = \frac{4}{3}b_v$. This is consistent with reference 4 which indicates that most of the increase in $C_{Y\beta}$ due to increasing horizontal-tail span occurs when the range of $\frac{b_h}{b_v}$ is from 0 to 1. For horizontal tails located in the mid position, the calculated values of $C_{Y\beta}$ indicated a negligible effect of root-chord ratio and horizontal-tail span.

The calculated rolling-moment derivatives, $(C_{l\beta})_v$ and $(C_{l\beta})_h$, and the total derivative $C_{l\beta}$ are presented in figure 7. It is apparent from this figure that the variation of the vertical-tail contribution $(C_{l\beta})_v$ with root-chord ratio $\frac{c_{r,h}}{c_{r,v}}$ is similar to the variation of $C_{Y\beta}$ with $\frac{c_{r,h}}{c_{r,v}}$ (fig. 6) and that most of the increase in the magnitude of $(C_{l\beta})_v$ due to end-plate effect was obtained when the root-chord ratio reached a value of 0.50. It is interesting to note that a similar condition exists for the horizontal-tail contribution $(C_{l\beta})_h$ when the horizontal tail has a span ratio $\frac{b_h}{b_v}$ of 4/3. This similarity does not exist for the horizontal-tail contribution at the larger horizontal-tail spans, however, and is primarily due to the large moment arms of the small loading on the outboard portions of the horizontal tail.

The large effect of root-chord ratio and horizontal-tail span on the total derivative $C_{l\beta}$ (fig. 7(c)) is due to the large effects of root-chord ratio and span on the horizontal-tail contribution $(C_{l\beta})_h$. For the largest span horizontal tail in the low position, the horizontal-tail contribution is large enough so that $C_{l\beta}$ is positive when root-chord ratios approach 1.0. Also of interest is the negligible variation of $C_{l\beta}$ with root-chord ratio for configurations having the shortest span horizontal tail in the low position. This negligible variation results because the horizontal-tail rolling moment almost cancelled the rolling moment due to end-plate effect on the vertical tail for all values of root-chord ratio considered.

Sideslip of horizontal tails with dihedral.- The additional loading on the tail surfaces due to horizontal-tail dihedral causes both the horizontal tail and the vertical tail to contribute to the lateral-force coefficient. The vertical-tail force is the result of an induced load and is, therefore, proportional to the dihedral angle. The horizontal-tail contribution to $C_{Y\beta}$ is caused primarily by the lateral tilt of the lift vectors through an angle equal to the dihedral angle. The vertical- and horizontal-tail contributions to the lateral-force derivative are presented in the forms $\left(\frac{C_{Y\beta}}{\Gamma}\right)_v$ and $\left(\frac{C_{Y\beta}}{\Gamma^2}\right)_h$, respectively, in figure 8. Increasing the root-chord ratio and horizontal-tail span increases the magnitude of $\left(\frac{C_{Y\beta}}{\Gamma}\right)_v$ for horizontal tails located at the extremities of the vertical tail but has a negligible influence on $\left(\frac{C_{Y\beta}}{\Gamma}\right)_v$ when the horizontal tail is at the mid position. The effect of horizontal-tail position shown in figure 8(a) is due to the opposite direction of the induced load for portions of the vertical tail above and below the horizontal tail. Although $\left(\frac{C_{Y\beta}}{\Gamma}\right)_v$ for horizontal tails in the mid position is almost invariant with root-chord ratio and horizontal-tail span, these effects did provide large changes on the span load coefficients (fig. 4(a)). In addition, horizontal-tail position has a negligible effect on the horizontal-tail contribution $\left(\frac{C_{Y\beta}}{\Gamma^2}\right)_h$, and increases in root-chord ratio or horizontal-tail span increase the magnitude of $\left(\frac{C_{Y\beta}}{\Gamma^2}\right)_h$ at all three vertical locations of the horizontal tail.

The rolling-moment contributions of the vertical- and horizontal-tail surfaces $\left(\frac{C_{l\beta}}{\Gamma}\right)_v$ and $\left(\frac{C_{l\beta}}{\Gamma}\right)_h$, respectively, are presented in figures 9(a) and 9(b), and the total derivative $\frac{C_{l\beta}}{\Gamma}$ is presented in figure 9(c). An examination of figures 9(a) and 9(b) indicates that root-chord ratio and horizontal-tail span influence both the horizontal- and vertical-tail rolling-moment derivatives: $\left(\frac{C_{l\beta}}{\Gamma}\right)_h$ and $\left(\frac{C_{l\beta}}{\Gamma}\right)_v$, respectively; whereas, horizontal-tail position appears to influence only

the vertical-tail derivative $\left(\frac{C_{l\beta}}{\Gamma}\right)_v$. The magnitude of the total derivative $\frac{C_{l\beta}}{\Gamma}$ is principally that of the horizontal tail for configurations having the larger span horizontal tails. The vertical-tail contribution only becomes a significant proportion of the total rolling-moment derivative when the horizontal tail has a span ratio of about $4/3$ or less.

Steady roll.- The calculated values of the lateral force due to steady roll for the various tail assemblies are presented in figure 10. The derivative C_{Y_p} arises, of course, only from the loads carried by the vertical tail. A comparison of the results for the horizontal tails located in the low and high positions shows that C_{Y_p} becomes more positive with an increase in root-chord ratio and horizontal-tail span for horizontal tails in the low position and more negative for horizontal tails in the high position. Of interest in figure 10 is the reversal in the sign of C_{Y_p} for the largest span horizontal tail in the low position when the root-chord ratio is of the order of 0.70 or larger. This reversal in load for the largest span horizontal tail and the negligible root-chord-ratio effect for the shortest span horizontal tail in the low position have been discussed previously. For horizontal tails located at the mid position, increases in root-chord ratio and horizontal-tail span have a negligible effect on C_{Y_p} .

The calculated values for the various tail assemblies for the damping in roll contributed by the vertical tail, the horizontal tail, and the complete tail assembly are presented in figure 11. Changes in root-chord ratio and horizontal-tail span influence not only the horizontal-tail contribution $(C_{l_p})_h$ but also the vertical-tail contribution $(C_{l_p})_v$. An examination of figure 11 indicates that, for most of the root-chord-ratio range considered, the horizontal tail provides the dominant contribution to the total derivative C_{l_p} when the horizontal tail has a span more than about twice as large as the vertical-tail span. For such configurations, the vertical-tail contribution becomes an appreciable part of the total C_{l_p} only when the root-chord ratio approaches zero. For configurations having horizontal tails of shorter spans $\left(\frac{b_h}{b_v} \text{ less than about } 2\right)$, the vertical-tail contribution to the total C_{l_p} is significant for all values of root-chord ratio.

CONCLUDING REMARKS

Subsonic span loads and the resulting stability derivatives have been calculated using the discrete-horseshoe-vortex method for a systematic series of isolated tail assemblies in sideslip and in steady roll to determine the effect of varying the chord of the horizontal tail. The incremental load due to horizontal-tail dihedral angle for the sideslip case was also computed for the various tail assemblies. The investigation covered variations in horizontal-tail chord, horizontal-tail span, and vertical location of the horizontal tail for an isolated tail assembly having a vertical tail of aspect ratio 1.0. Each tail surface considered had a taper ratio of 0.5 and an unswept quarter-chord line. The results of the investigation are presented in figures from which the span loads and the resulting stability derivatives can be obtained.

The results of this paper showed trends that were in agreement with the results of previous investigations for variations in horizontal-tail span and vertical location of the horizontal tail. Variations in horizontal-tail chord expressed herein in terms of the root-chord ratio, the ratio of horizontal-tail root chord to vertical-tail root chord, were found to have a pronounced influence on most of the span loads and the resulting stability derivatives. For most of the cases considered, the rate of change of the span load coefficients and the stability derivatives with the root-chord ratio was found to be a maximum for small values of root-chord ratio and to decrease as root-chord ratio increased.

Langley Research Center,
National Aeronautics and Space Administration,
Langley Field, Va., January 7, 1969.

REFERENCES

1. Katzoff, S., and Mutterperl, William: The End-Plate Effect of a Horizontal-Tail Surface on a Vertical-Tail Surface. NACA TN 797, 1941.
2. Murray, Harry E.: Wind-Tunnel Investigation of End-Plate Effects of Horizontal Tails on a Vertical Tail Compared With Available Theory. NACA TN 1050, 1946.
3. Riley, Donald R.: Effect of Horizontal-Tail Span and Vertical Location on the Aerodynamic Characteristics of an Unswept Tail Assembly in Sideslip. NACA Rep. 1171, 1954. (Supersedes NACA TN 2907.)
4. Queijo, M. J., and Riley, Donald R.: Calculated Subsonic Span Loads and Resulting Stability Derivatives of Unswept and 45° Sweptback Tail Surfaces in Sideslip and in Steady Roll. NACA TN 3245, 1954.
5. Campbell, George S.: A Finite-Step Method for the Calculation of Span Loadings of Unusual Plan Forms. NACA RM L50L13, 1951.
6. Gray, W. L., and Schenk, K. M.: A Method for Calculating the Subsonic Steady-State Loading on an Airplane With a Wing of Arbitrary Plan Form and Stiffness. NACA TN 3030, 1953.

TABLE I.- TAIL SURFACE FOR WHICH SPAN LOADS AND DERIVATIVES WERE CALCULATED

[Each surface has a taper ratio of 0.5]

(a) $\frac{c_{r,h}}{c_{r,v}} = 1.00$

(b) $\frac{c_{r,h}}{c_{r,v}} = 0.75$

Horizontal tail	$\frac{b_h}{b_v}$	A_h
	4	4.0000
	$\frac{8}{3}$	2.6667
	$\frac{4}{3}$	1.3333

Horizontal tail	$\frac{b_h}{b_v}$	A_h
	4	5.3333
	$\frac{8}{3}$	3.5556
	$\frac{4}{3}$	1.7778

(c) $\frac{c_{r,h}}{c_{r,v}} = 0.50$

(d) $\frac{c_{r,h}}{c_{r,v}} = 0.25$

Horizontal tail	$\frac{b_h}{b_v}$	A_h
	4	8.0000
	$\frac{8}{3}$	5.3333
	$\frac{4}{3}$	2.6667

Horizontal tail	$\frac{b_h}{b_v}$	A_h
	4	16.0000
	$\frac{8}{3}$	10.6667
	$\frac{4}{3}$	5.3333

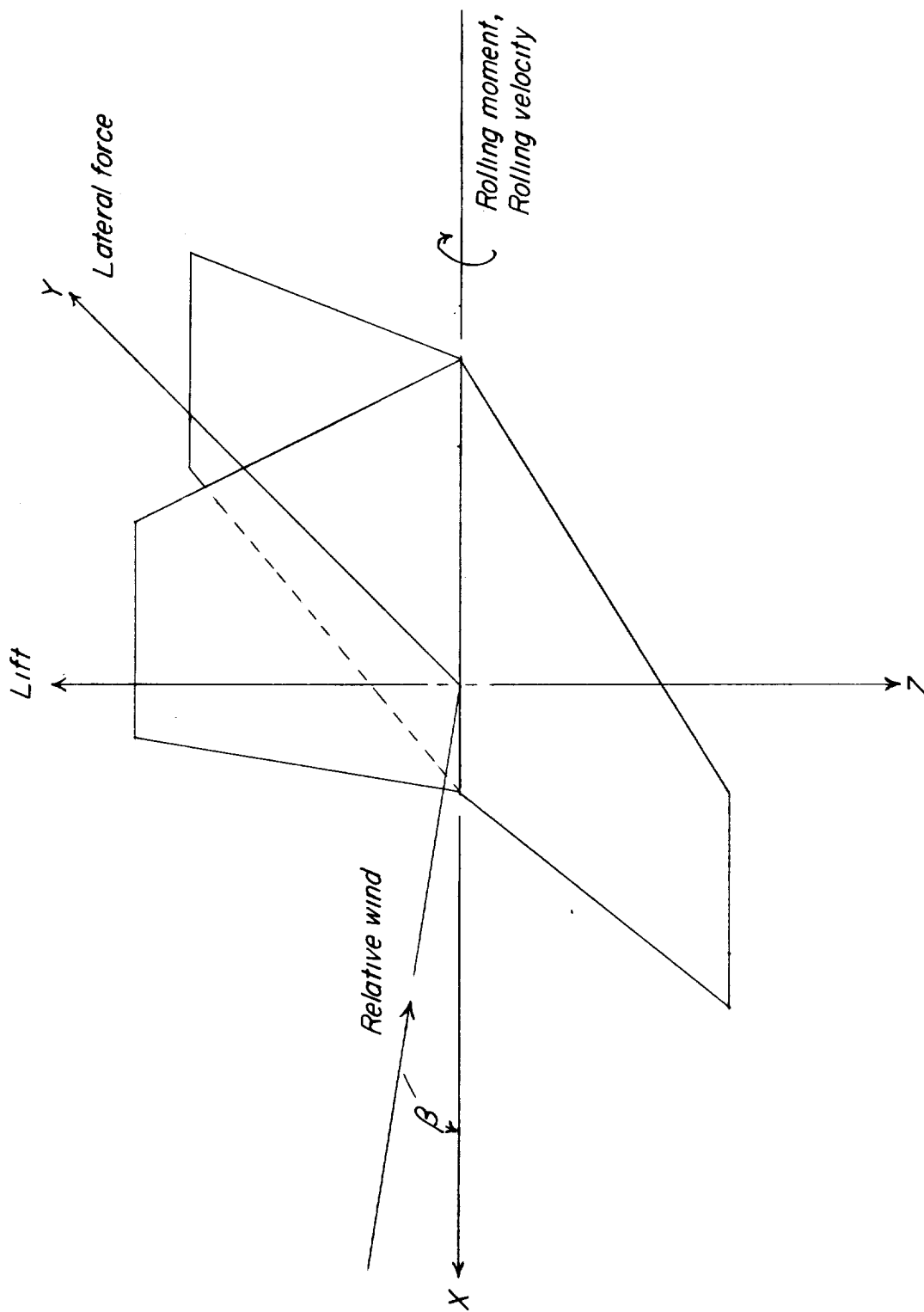


Figure 1.- System of axes used.

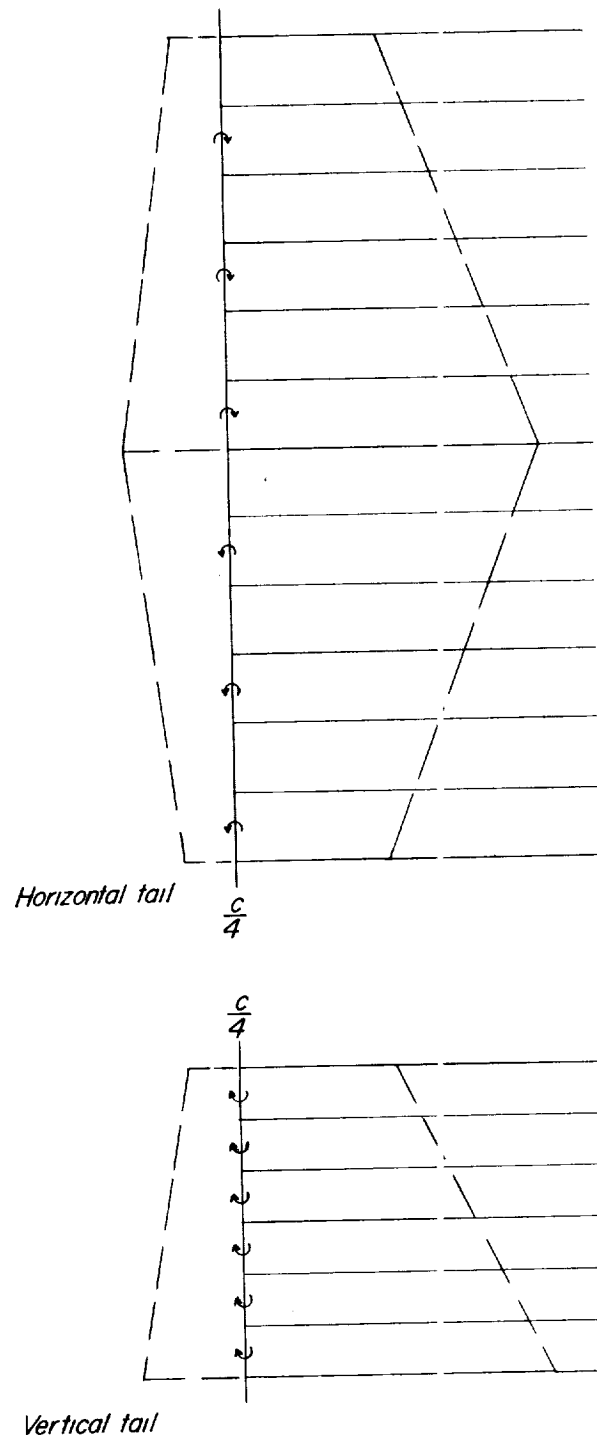
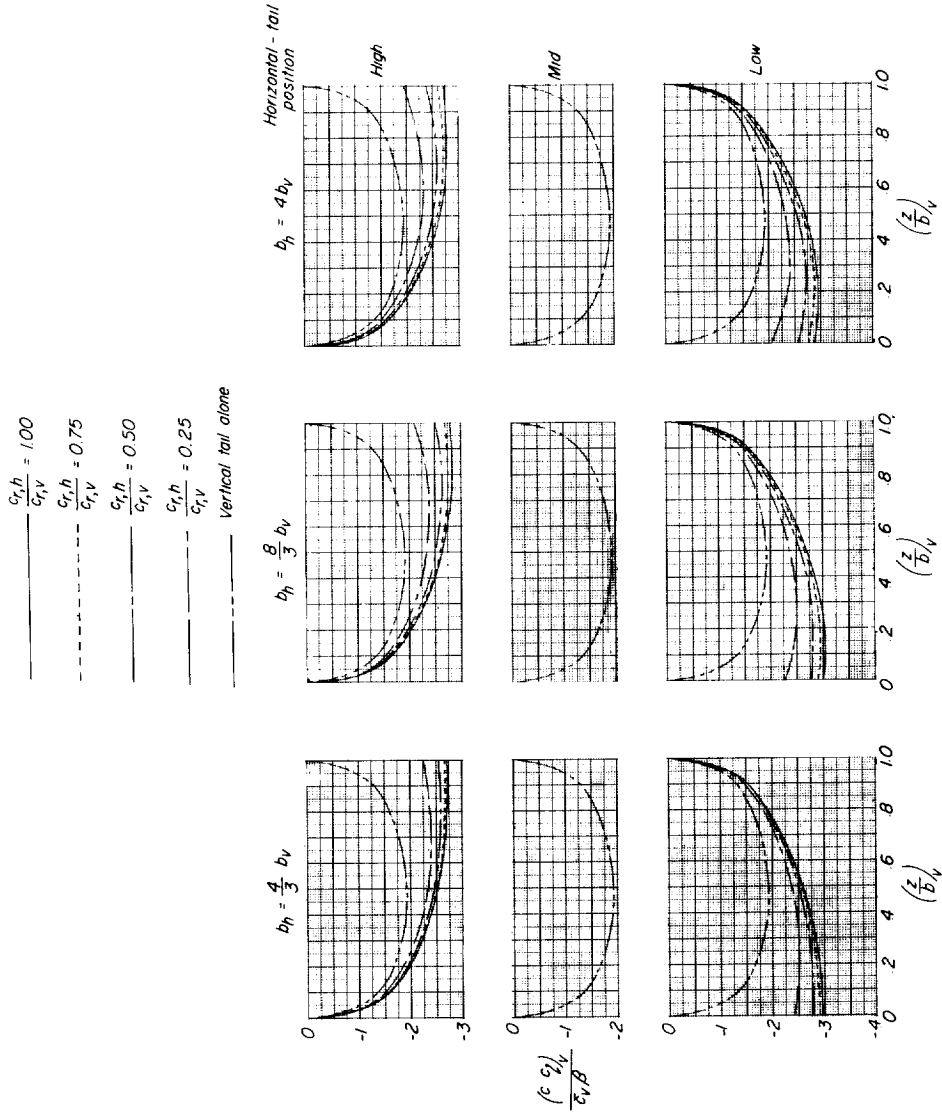
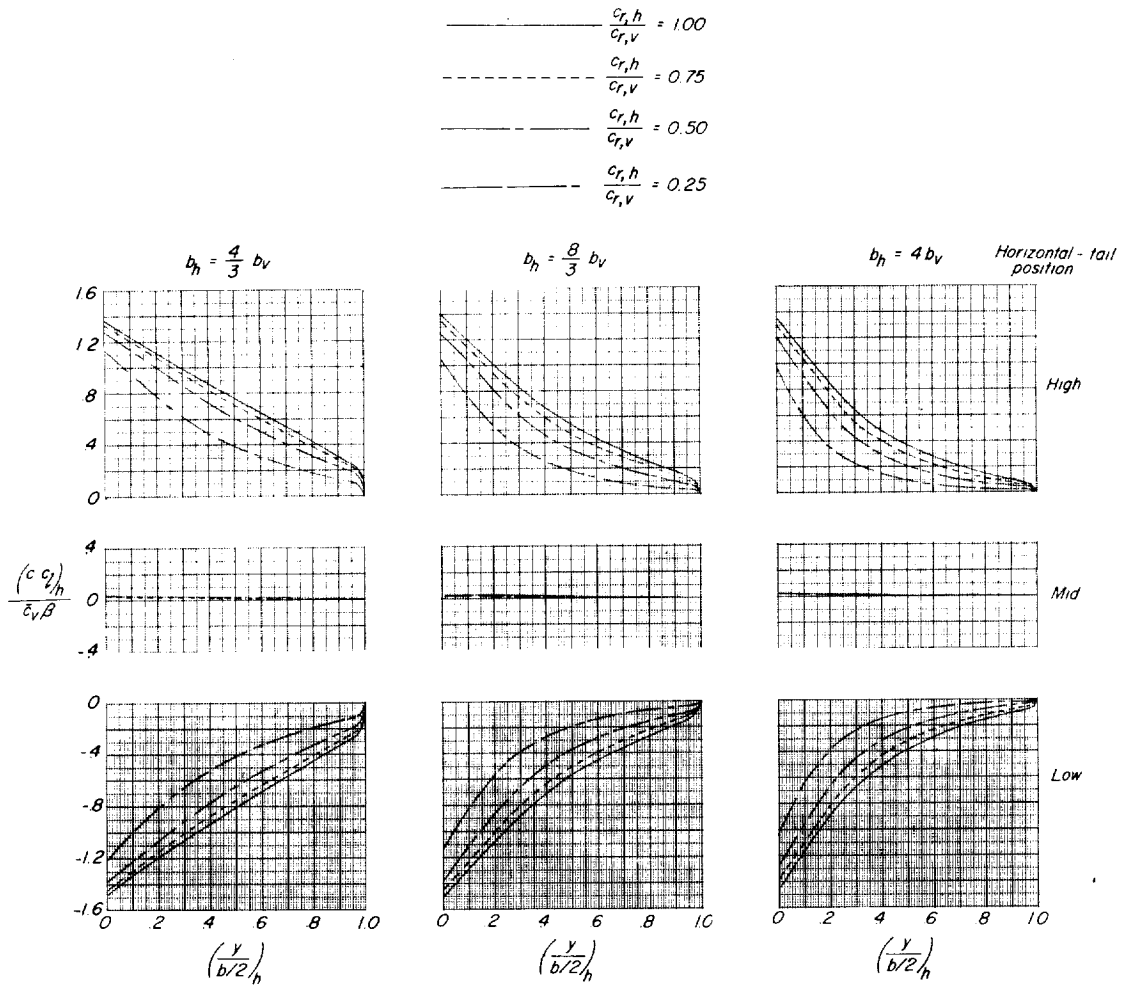


Figure 2.- Representation of tail surfaces by finite-step horseshoe vortices.



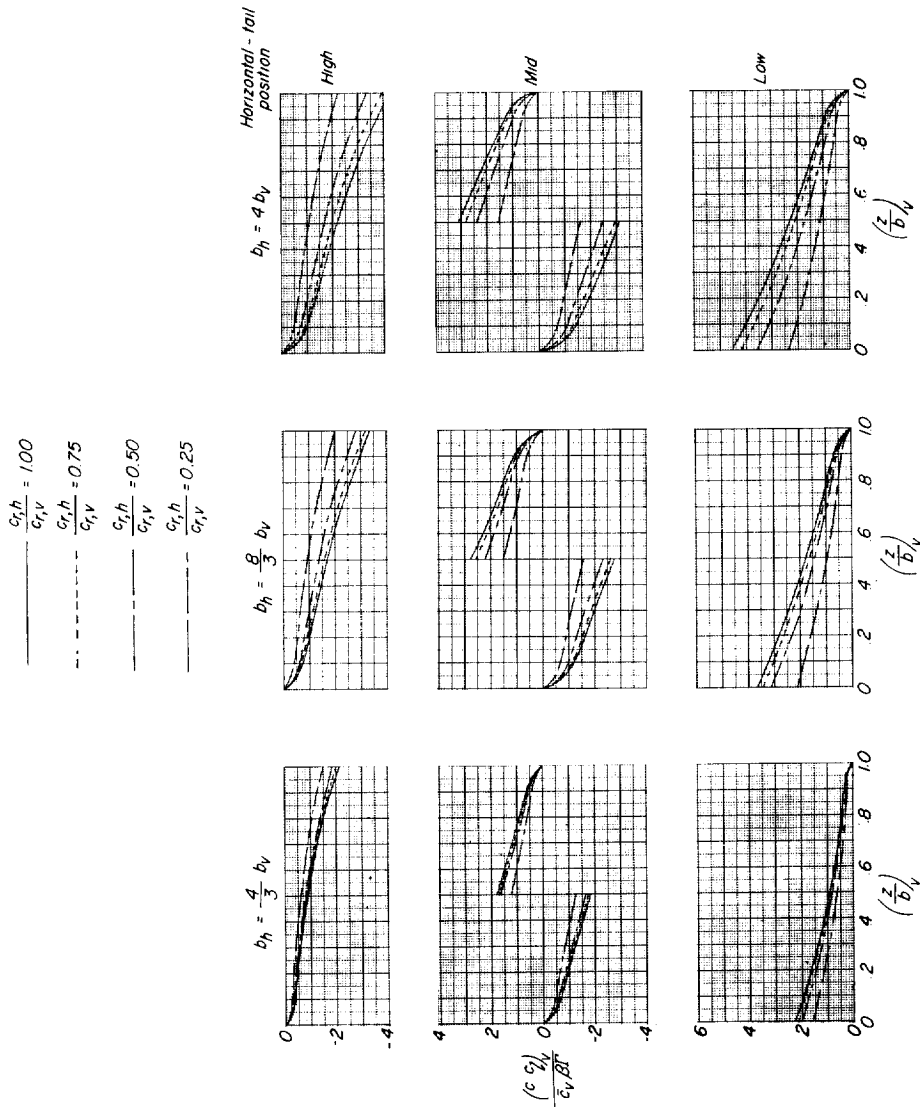
(a) Loads on vertical surfaces.

Figure 3.- Calculated span loads for tail assemblies in sideslip. $\Gamma = 0$.



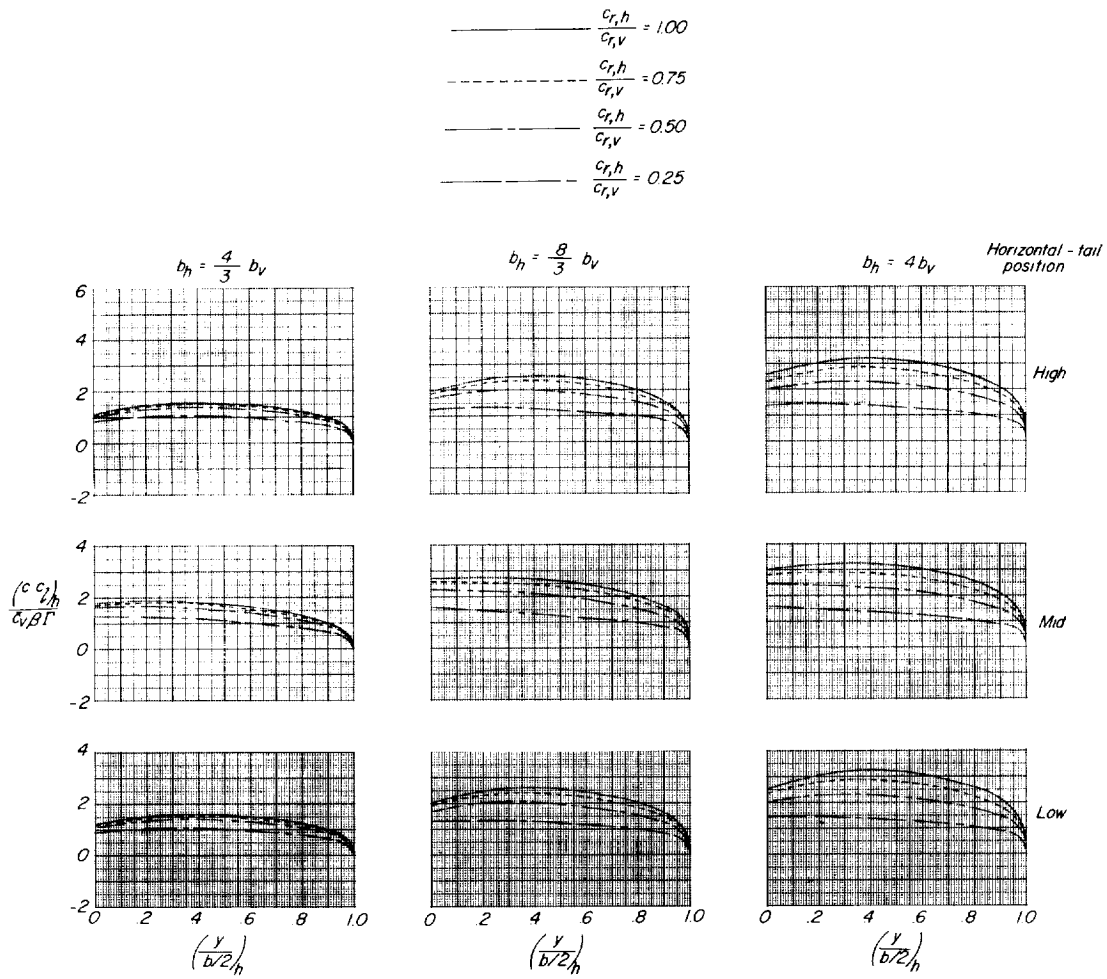
(b) Induced loads on horizontal surfaces.

Figure 3.- Concluded.



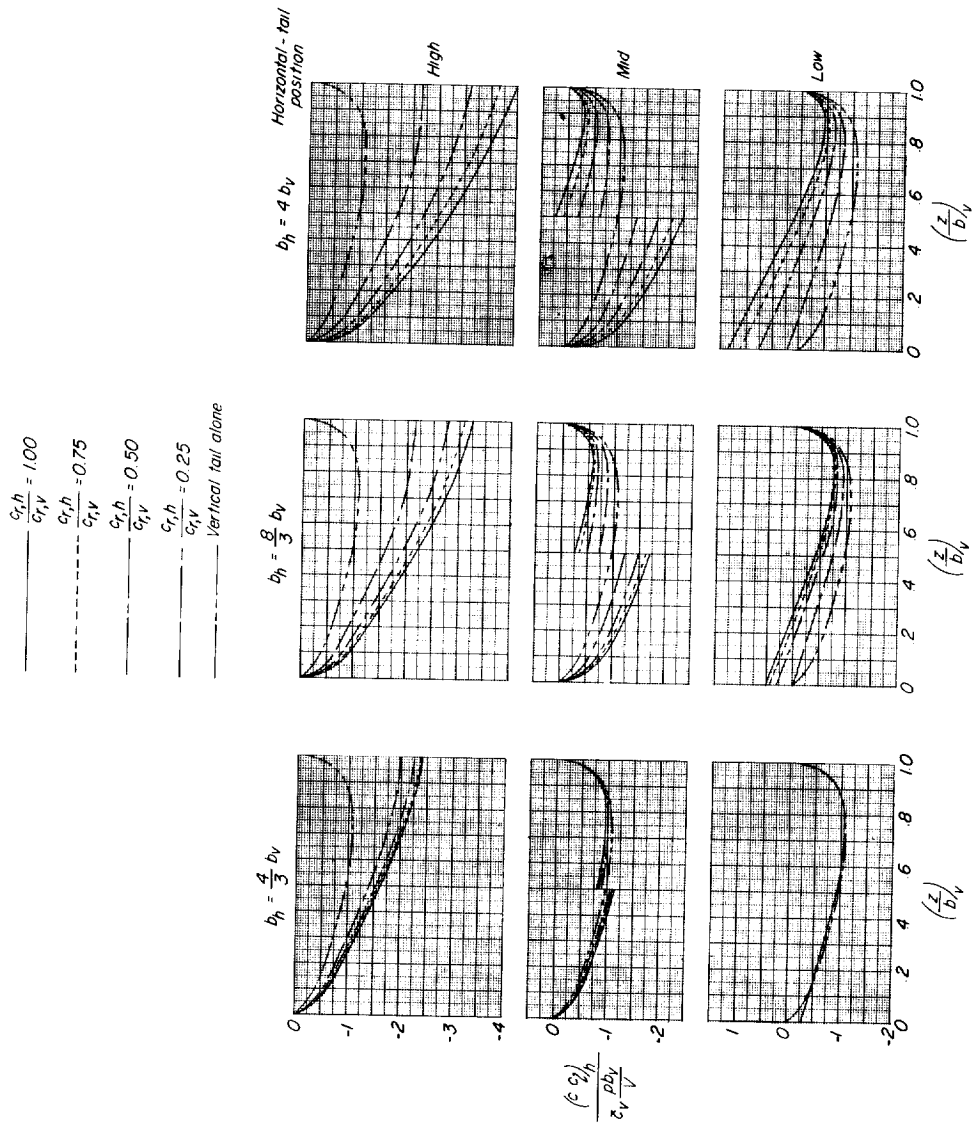
(a) Induced loads on vertical surfaces.

Figure 4.- Calculated span loads due to horizontal-tail dihedral angle for tail assemblies in sideslip.



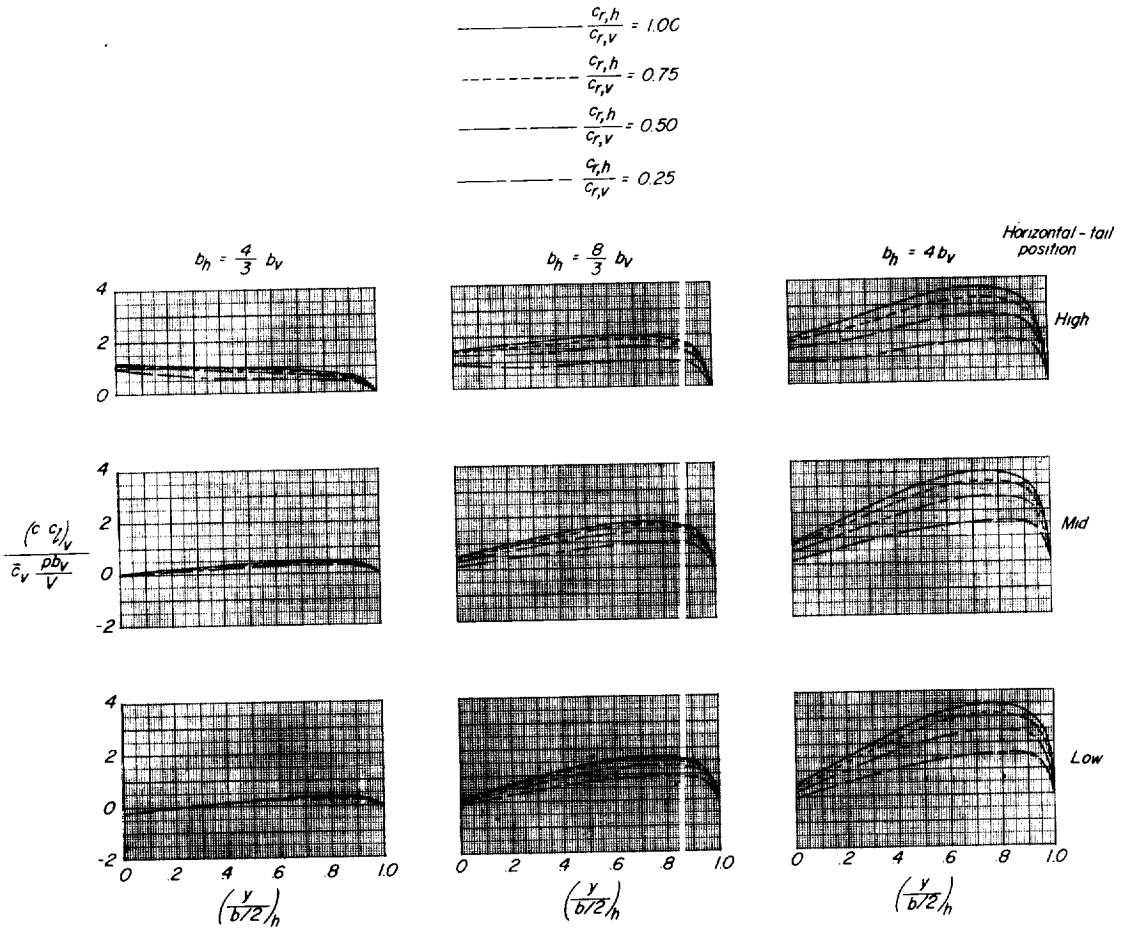
(b) Loads on horizontal surfaces.

Figure 4.- Concluded.



(a) Loads on vertical surfaces.

Figure 5.- Calculated span loads for tail assemblies in steady roll. $\Gamma = 0$.



(b) Loads on horizontal surfaces.

Figure 5.- Concluded.

$$\begin{array}{l} \text{----- } b_h = \frac{4}{3} b_v \\ \text{----- } b_h = \frac{8}{3} b_v \\ \text{----- } b_h = 4 b_v \end{array}$$

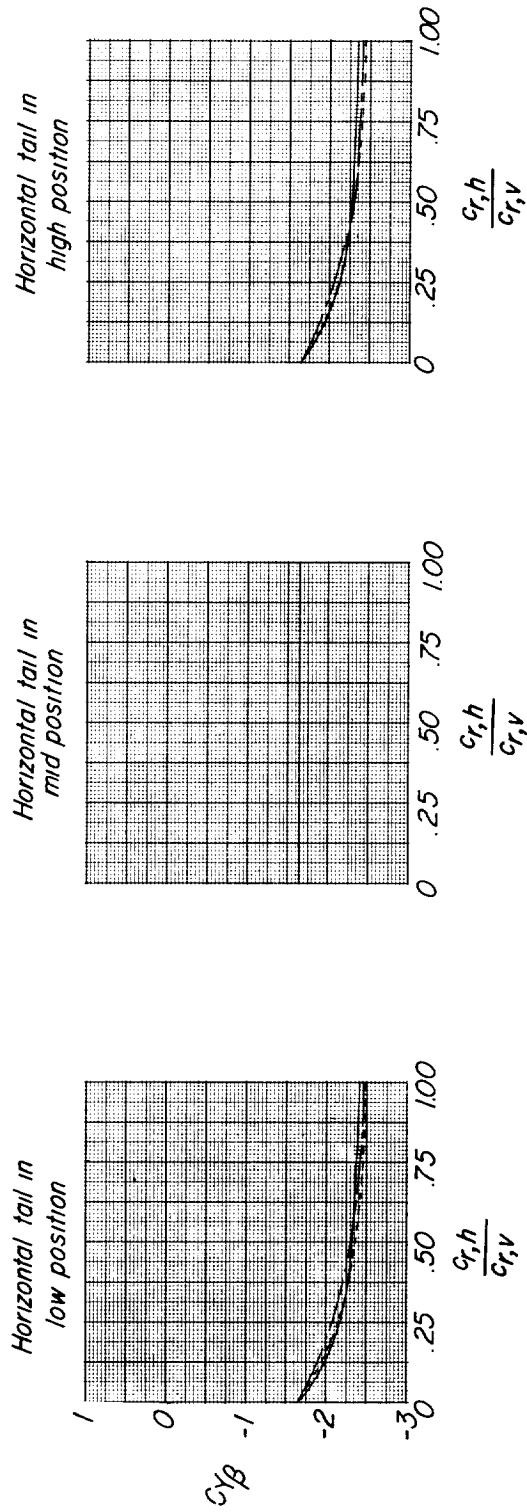
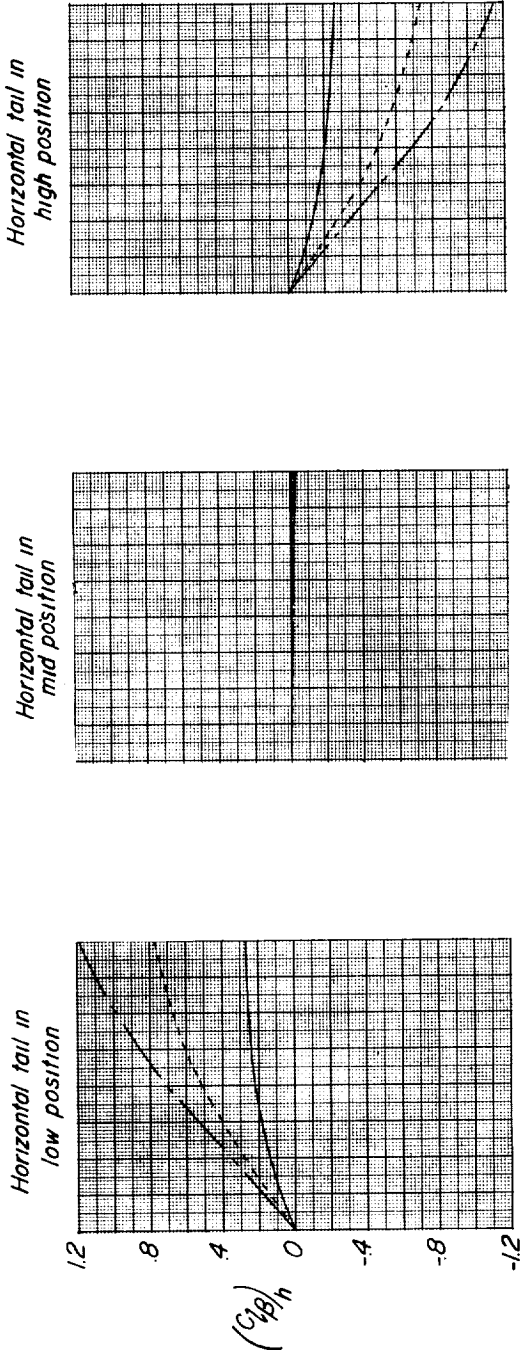
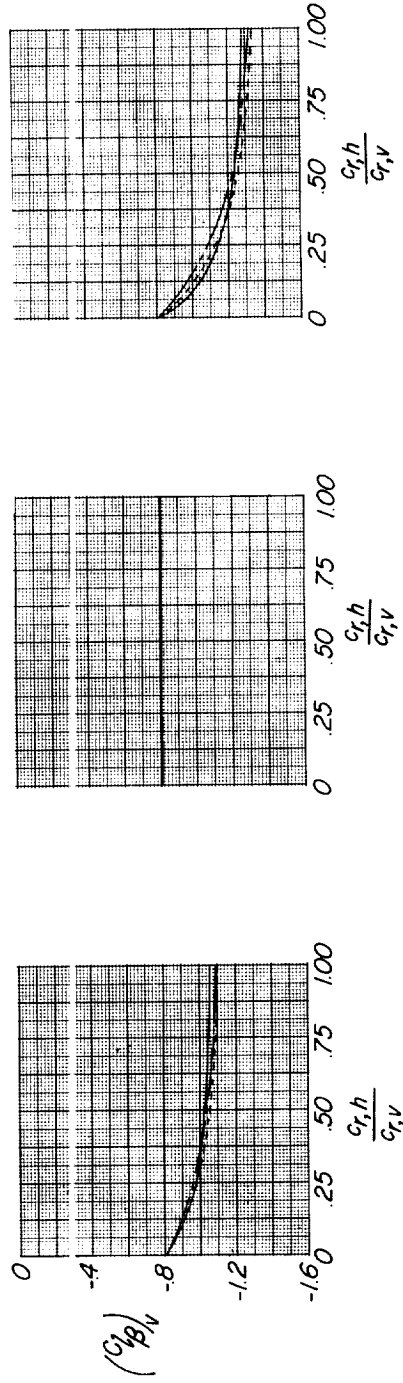


Figure 6.- Effect of root-chord ratio, horizontal-tail position, and horizontal-tail span on the calculated values of $C_{y\beta}$ for various tail assemblies. $\Gamma = 0$.

$\text{---} b_h = \frac{4}{3} b_v$
 $\text{- - -} b_h = \frac{8}{3} b_v$
 $\text{---} b_h = 4 b_v$



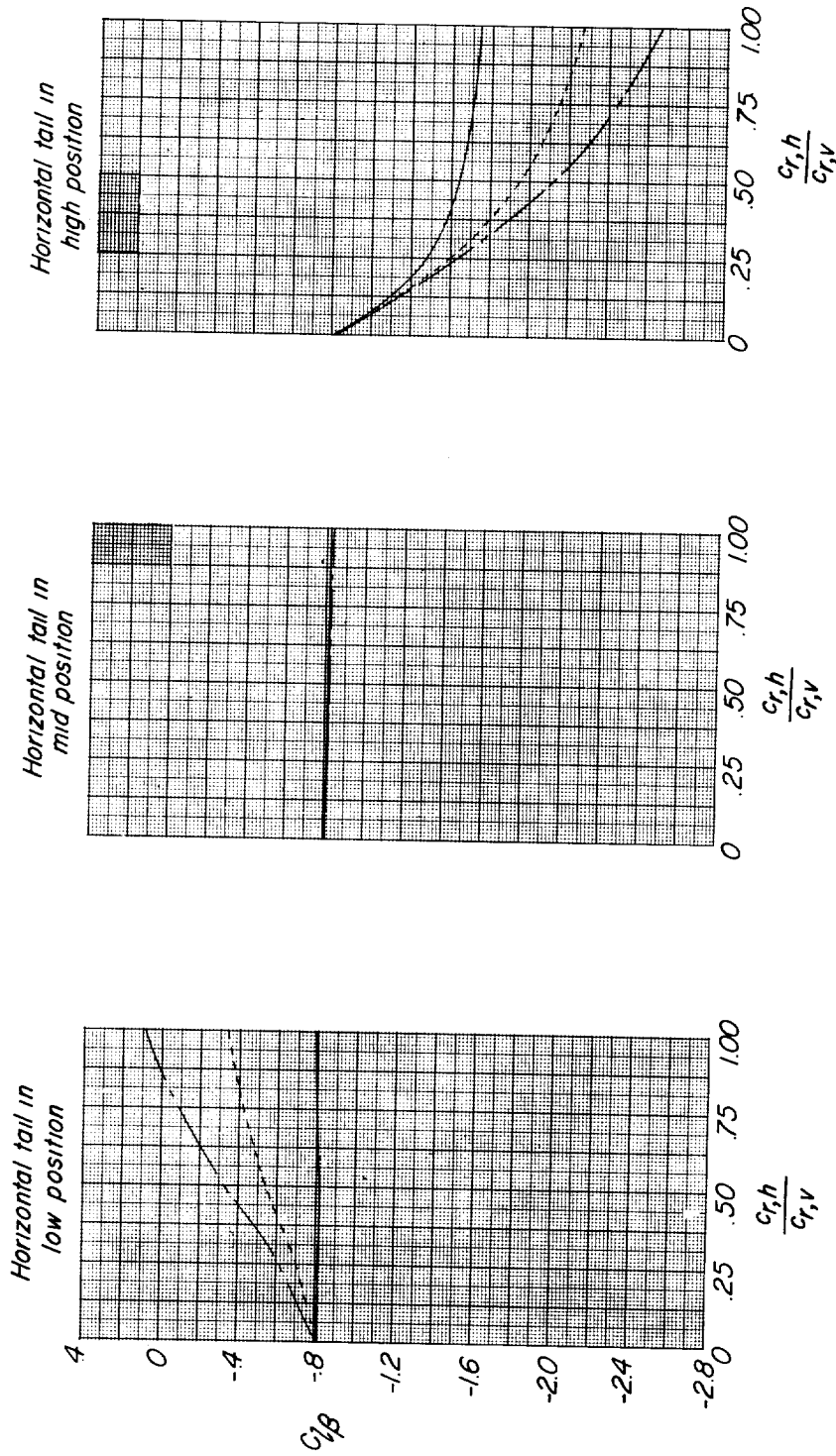
(a) Horizontal-tail contribution.



(b) Vertical-tail contribution.

Figure 7.- Effect of root-chord ratio, horizontal-tail position, and horizontal-tail span on the calculated values of $C_{l\beta}$ for various tail assemblies. $\Gamma = 0$.

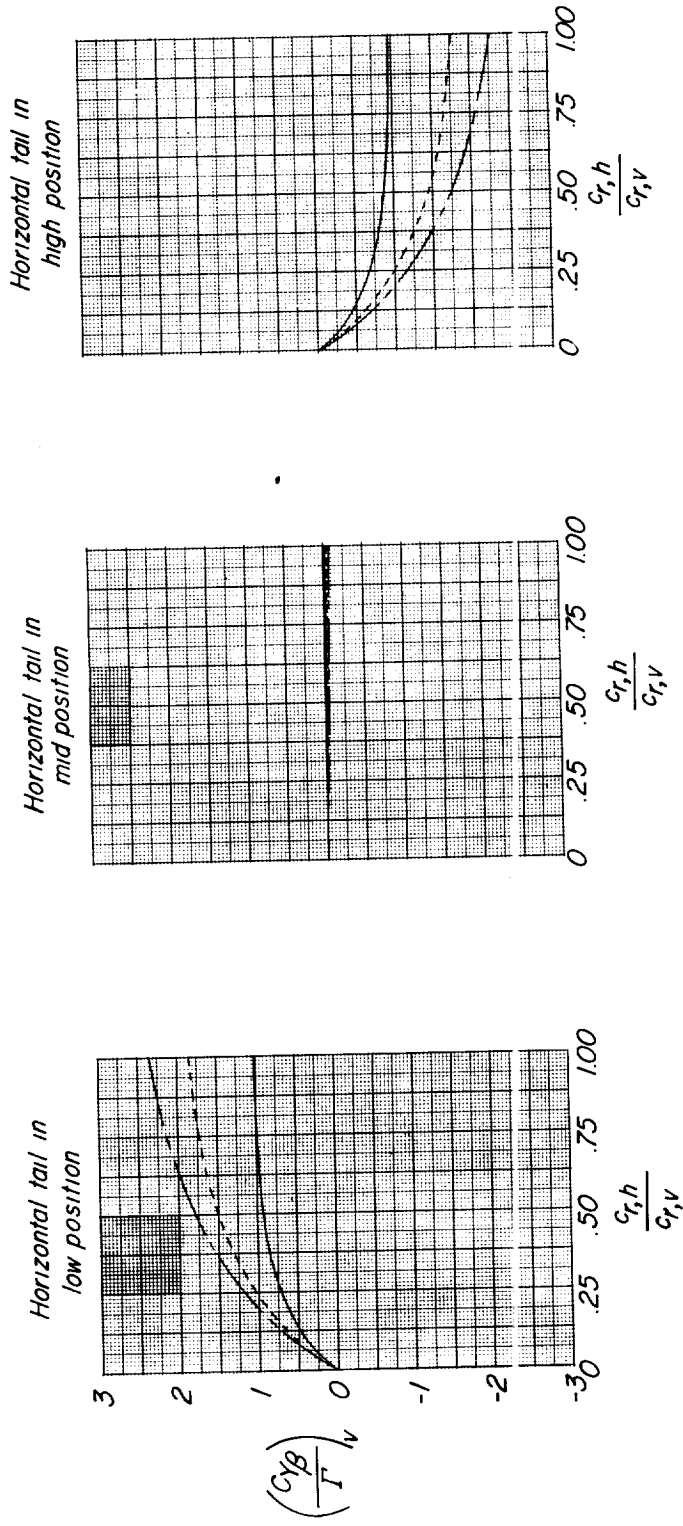
$\text{---} b_h = \frac{4}{3} b_v$
 $\text{- - -} b_h = \frac{8}{3} b_v$
 $\text{---} b_h = 4 b_v$



(c) Total $C_{l\beta}$.

Figure 7.- Concluded.

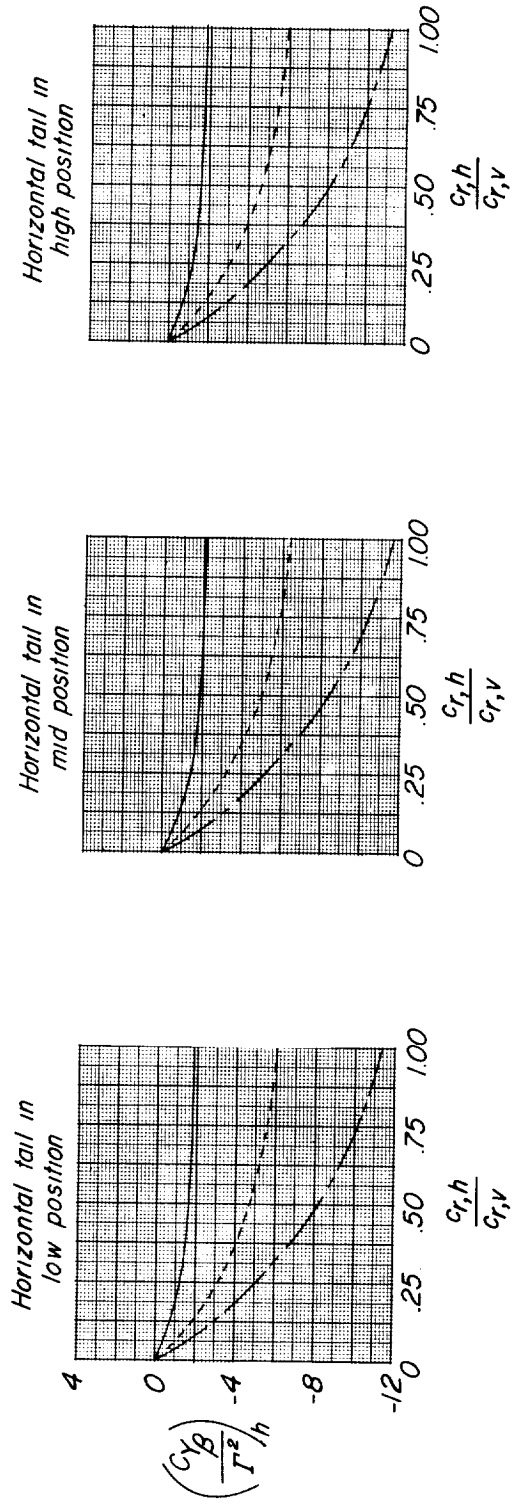
_____ $b_h = \frac{4}{3} b_v$
 - - - - - $b_h = \frac{8}{3} b_v$
 - - - - - $b_h = 4 b_v$



(a) Vertical-tail contribution.

Figure 8.- Effect of root-chord ratio, horizontal-tail position, and horizontal-tail span on the calculated values of $C_{Y\beta}$ due to horizontal-tail dihedral for various tail assemblies.

_____ $b_h = \frac{4}{3} b_v$
 - - - - - $b_h = \frac{8}{3} b_v$
 _____ $b_h = 4 b_v$



(b) Horizontal-tail contribution.

Figure 8.- Concluded.

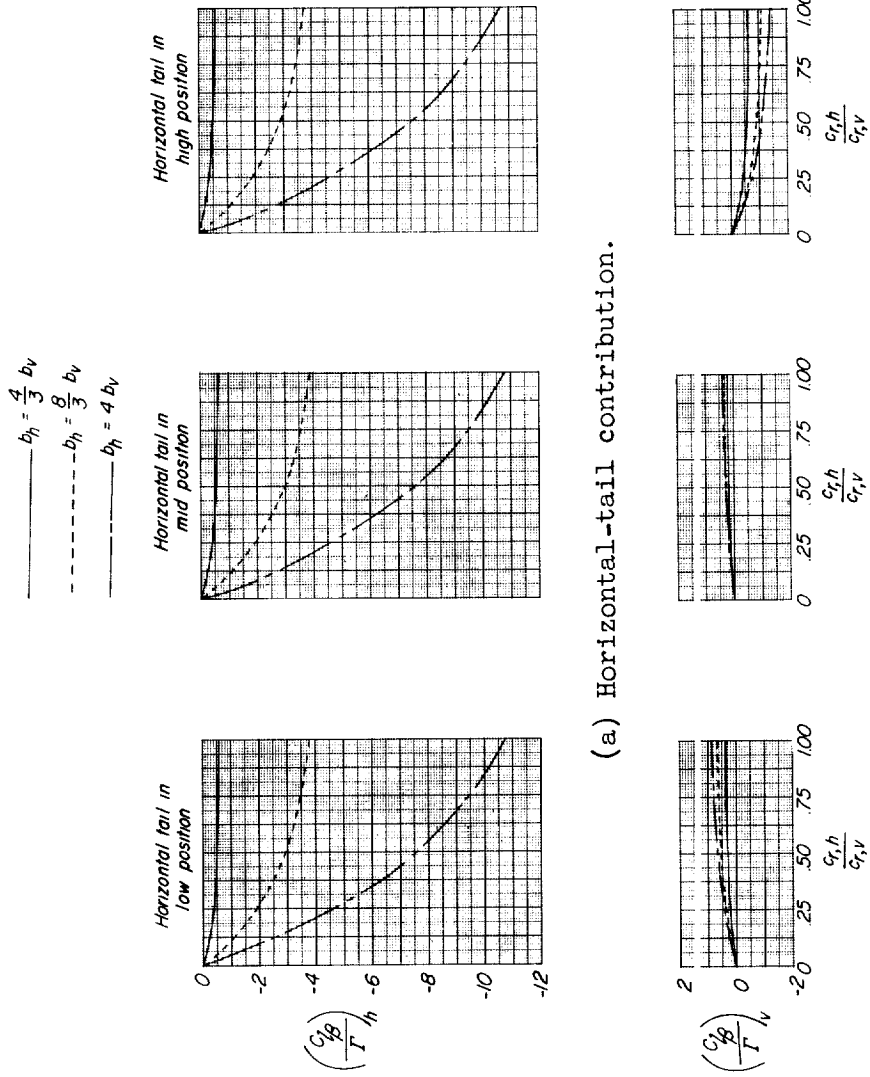
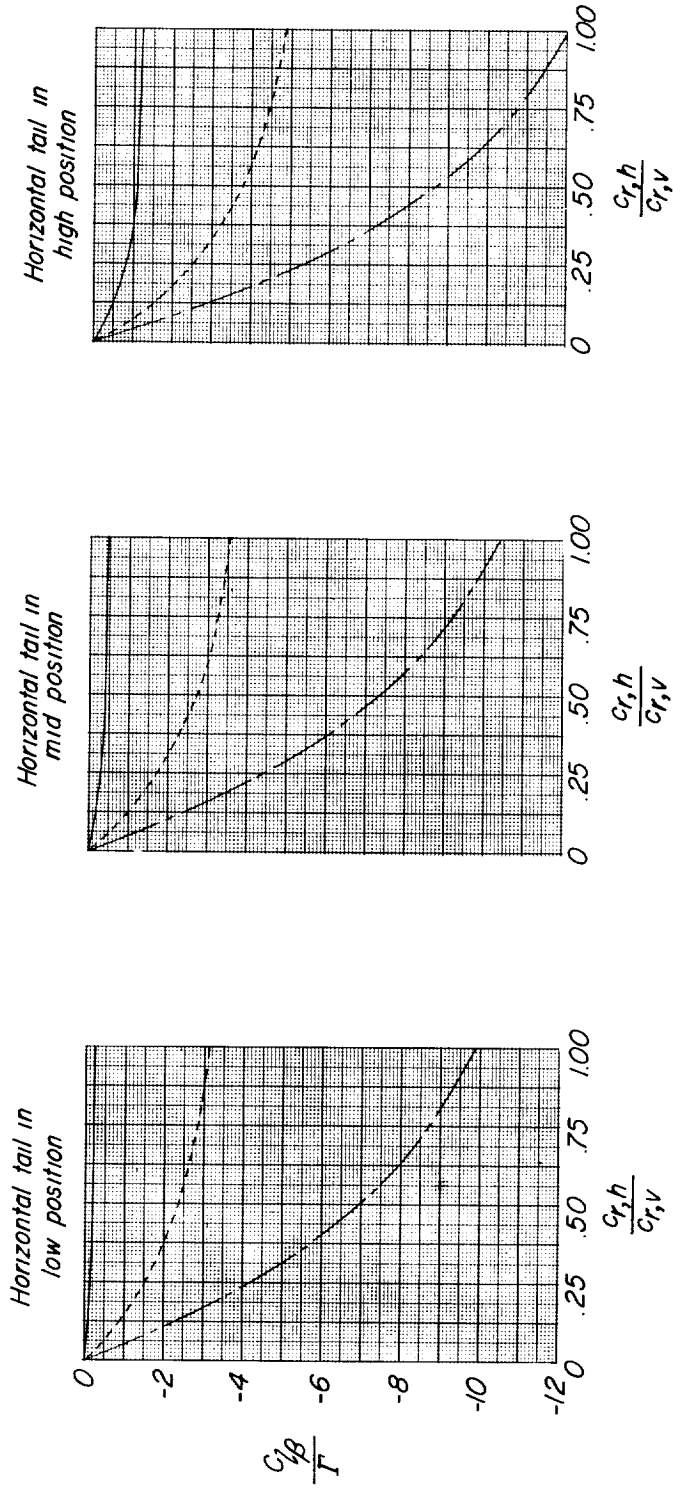


Figure 9.- Effect of root-chord ratio, horizontal-tail position, and horizontal-tail span on the calculated values of $C_{l\beta}$ due to horizontal-tail dihedral for various tail assemblies.

$\text{---} b_h = \frac{4}{3} b_v$
 $\text{- - -} b_h = \frac{8}{3} b_v$
 $\text{---} b_h = 4 b_v$



(c) Total $C_{1\beta}$.

Figure 9.- Concluded.

$\text{---} b_h = \frac{4}{3} b_v$
 $\text{- - -} b_h = \frac{8}{3} b_v$
 $\text{---} b_h = 4 b_v$

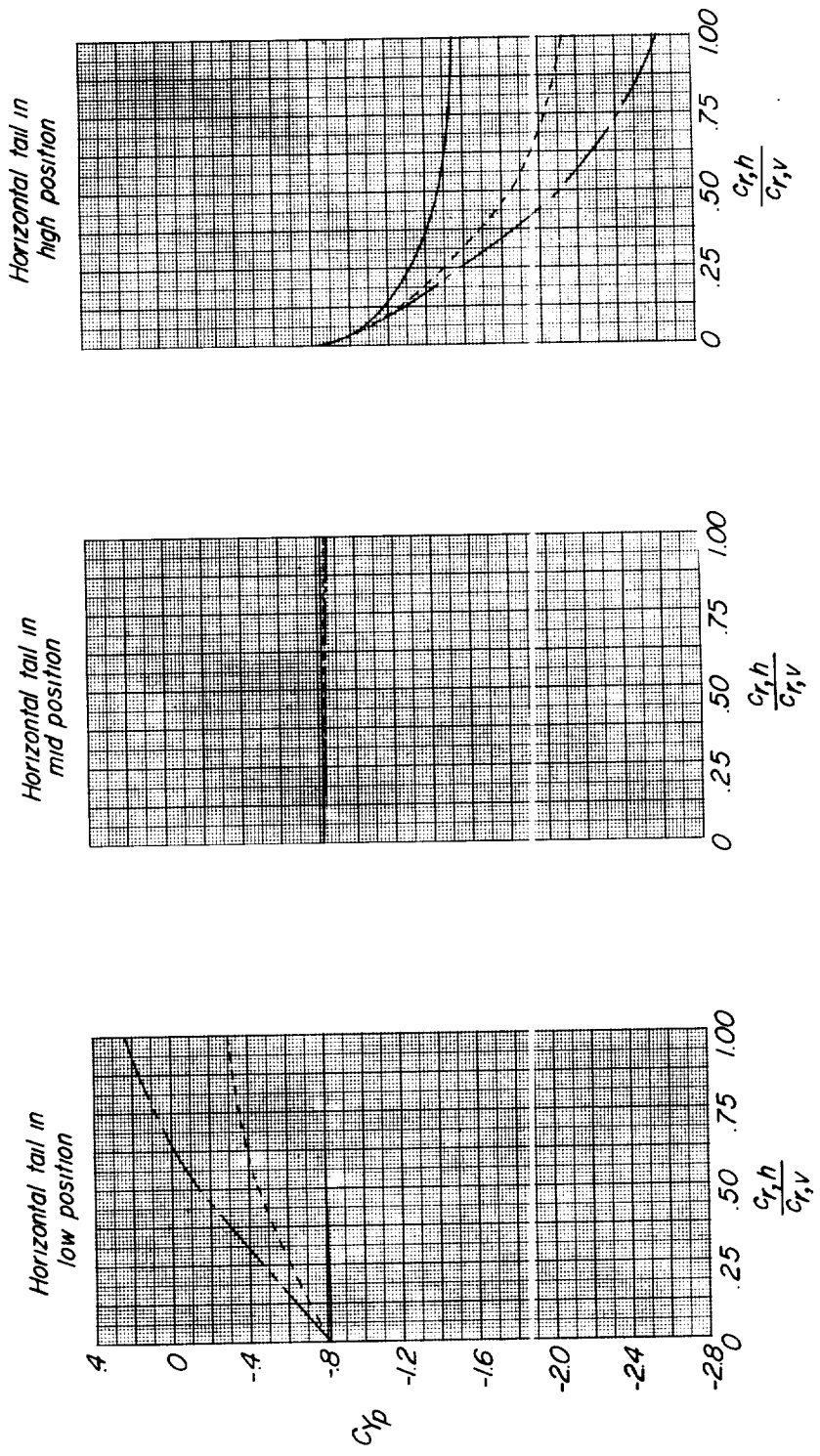
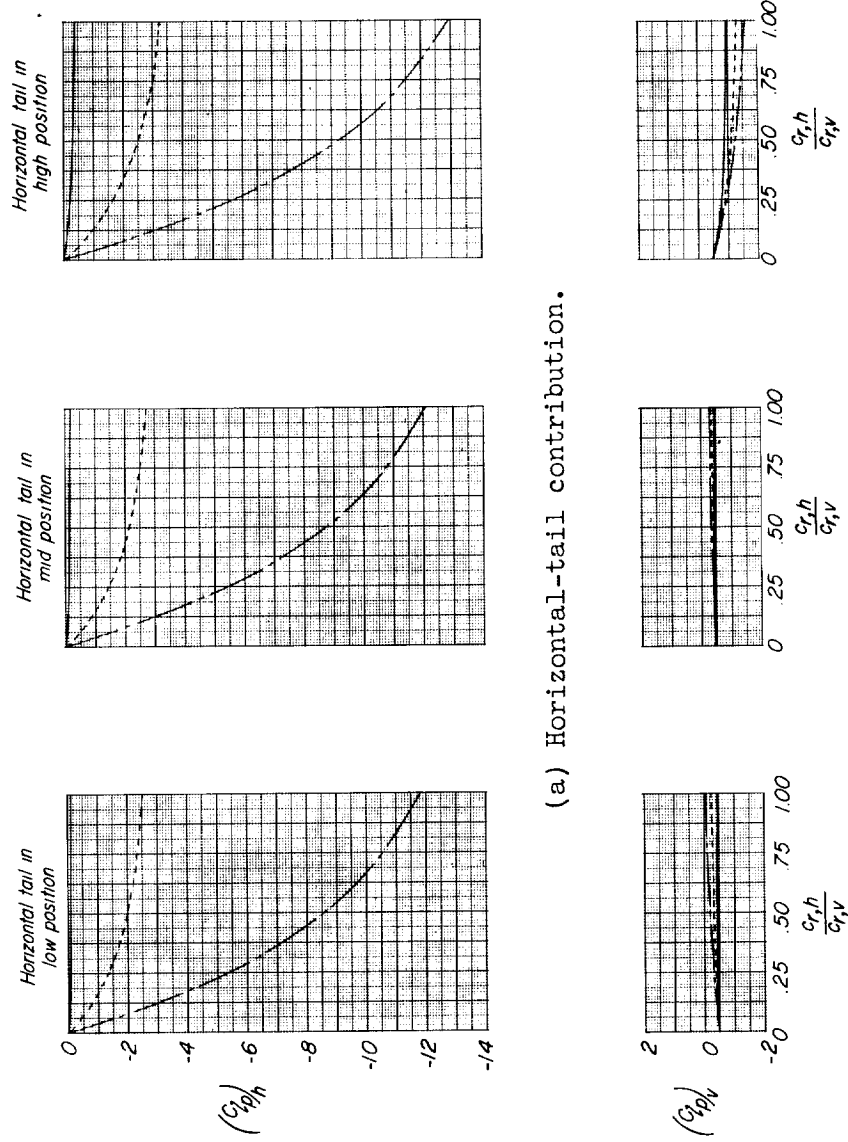


Figure 10.- Effect of root-chord ratio, horizontal-tail position, and horizontal-tail span on the calculated values of C_{Yp} for various tail assemblies. $\Gamma = 0$.

————— $b_h = \frac{4}{3} b_v$
 - - - - - $b_h = \frac{8}{3} b_v$
 ———— $b_h = 4 b_v$

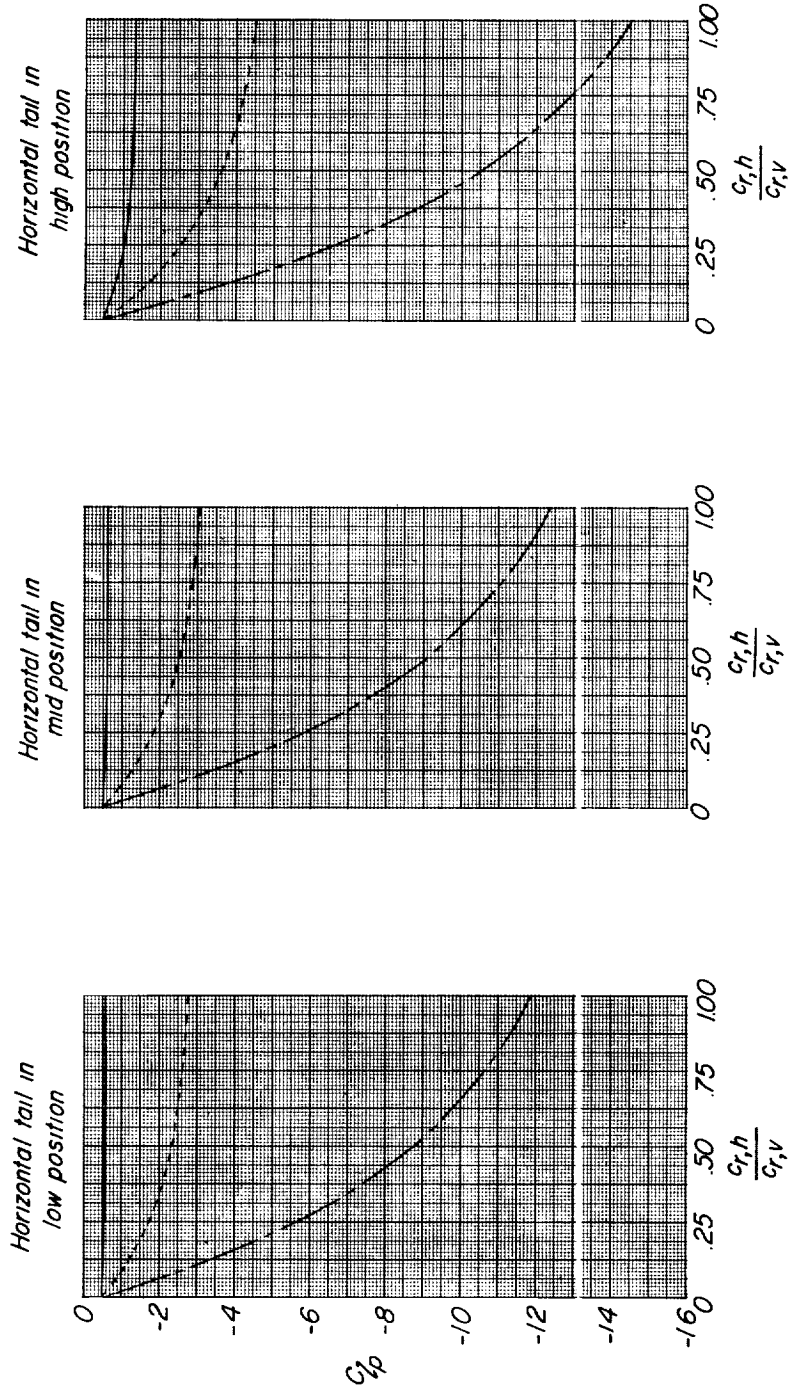


(a) Horizontal-tail contribution.

(b) Vertical-tail contribution.

Figure 11.- Effect of root-chord ratio, horizontal-tail position, and horizontal-tail span on the calculated values of C_{lp} for various tail assemblies. $\Gamma = 0$.

$\text{---} b_h = \frac{4}{3} b_v$
 $\text{- - -} b_h = \frac{8}{3} b_v$
 $\text{---} b_h = 4 b_v$



(c) Total C_{lp} .

Figure 11.- Concluded.